Research Article | Vol. 27, No. 5 | 4 Mar 2019 | OPTICS EXPRESS 6147
Optics EXPRESS

Ring resonator based polarization diversity WDM receiver

ANTHONY H. K. PARK,[1,*] HOSSAM SHOMAN,[1] MINGLEI MA,[1] SUDIP SHEKHAR,[1] AND LUKAS CHROSTOWSKI[1]

[1] *Department of Electrical and Computer Engineering, University of British Columbia, Vancouver, British Columbia V6T 1Z4, Canada*
[*] *park68@ece.ubc.ca*

Abstract: A ring resonator based 4 channel wavelength division multiplexing (WDM) receiver with polarization diversity is demonstrated at 10 Gb/s per channel. By forming a waveguide loop between the two output ports of a polarization splitter-rotator (PSR), the input signals in the quasi-transverse-electric (quasi-TE) and the quasi-transverse-magnetic (quasi-TM) polarizations can be demultiplexed by the same set of ring resonator filters, thus reducing the number of required channel control circuits by half compared to methods which process the two polarizations individually. Large signal measurement results indicate that the design can tolerate a signal delay of up to 30% of the unit interval (UI) between the two polarizations, which implies that compensating for manufacturing variability with optical delay lines on chip is not necessary for a robust operation. The inter-channel crosstalk is found negligible down to 0.4nm (50 GHz) spacing, at which point the adjacent channel isolation is 17 dB, proving the design's compatibility for dense WDM application.

1. Introduction

Silicon photonics has emerged as a promising candidate for low cost, high speed interconnects in data centers, due to its CMOS compatibility, low cost of production, and large-scale integration capability [1]. However, silicon-on-insulator (SOI) waveguides can suffer from strong polarization dependence due to their high mode confinement factor and rectangular cross-sections.

This is particularly troublesome for silicon photonic wavelength division multiplexing (WDM) receivers, where the performance of the channel filters changes with respect to the polarization of the optical input from a single mode fiber. Polarization-maintaining fibers can be used to keep the input in a single polarization state, but they are expensive to deploy in commercial applications [2]. Instead, polarization can be managed on the receiver chip by using polarization splitters and rotators available in the silicon photonics platform [3–6].

One can use a polarization splitter to separate the input beam into two paths, and place channel filters on each path, to later combine the signals at the photodetector (PD). The channel filters may comprise of cascaded Mach Zehnder interferometers (MZIs) [7] or ring resonators [2, 8], and their relevant publication results are shown in Table 1, listing their filter type, bit rate, polarization-dependent loss (PDL), and insertion loss.

Alternatively, one can reduce the number of channel filters by simply placing a polarization rotator in one of the paths, and then connecting it back to the other path to form a loop, such that the two signals can counter-propagate along the same waveguide path in the same polarization [10, 11]. Silicon nitride based arrayed-waveguide grating (AWG) has been implemented using this polarization diversity method, but suffers from high insertion loss [9]. Ring resonators are geometrically compatible with this method, which has recently been further expanded as a polarization and wavelength division demultiplexer in [12]. However, to the best of our knowledge, the operation of a multi-channel WDM receiver with integrated PDs based on the loop method with ring resonator filters has not been demonstrated yet.

#353364 https://doi.org/10.1364/OE.27.006147
Journal © 2019 Received 14 Dec 2018; revised 24 Jan 2019; accepted 30 Jan 2019; published 20 Feb 2019

Optics EXPRESS

Table 1. Polarization diversity receiver examples

Reference	Filter type	Bit rate	PDL	Insertion loss
[7]	MZI	4 x 10 Gb/s	< 0.9 dB	6.2 dB
[8]	ring	5 x 20 Gb/s	< 0.5 dB	7.8 dB
[2]	ring	4 x 25 Gb/s	< 0.5 dB	6.6 dB
[9]	AWG	10 x 10 Gb/s	< 1.8 dB	13.5 dB
This work	ring	4 x 10 Gb/s	1.0 dB	7.5 dB

In this paper, for the first time, we experimentally demonstrate the operation of a 4 channel WDM polarization insensitive receiver based on the loop design with ring resonator filters. Large signal measurements are made at 10 Gb/s per channel to evaluate the performance at different input polarizations. For practicality assessment, the impact of interchannel crosstalk at DWDM grid spacing and its operational tolerance against mismatches in the length of the signal path are evaluated.

2. Device design

The schematic of the receiver is shown in Fig. 1. An edge coupler is used to couple the horizontally (h) and vertically (v) polarized components of a light source from an optical fiber into the quasi-transverse-electric (quasi-TE) and the quasi-transverse-magnetic (quasi-TM) modes in the waveguide, respectively. We will refer to these two modes simply as the "TE" mode and the "TM" mode for the rest of this paper. The two orthogonal modes in the waveguide are then separated into two paths by a polarization splitter-rotator (PSR). The TE mode input passes through the first path (herein called the 'TE path') as a TE mode, and the TM mode input rotates and passes through the second path (herein called the 'TM path') as a TE mode. The two paths are connected into a loop, along which four add-drop ring resonator filters are placed. In this work, the mode evolution based PSR as described in [13] is used. The drop ports of the rings are connected to on-chip PDs.

Compared to polarization diversity circuits presented in [2, 14], this design requires half as many control circuits corresponding to the halved number of microring resonator filters. As the outputs of the PSR are counter-propagating with respect to each other, they do not cause interference unless there is a backscattering element which couples the two paths.

One potential performance concern in this design relates to the length difference between the TE path and the TM path leading to each PD. For example, in Fig. 1, because the signal in TM path arrives at the channel 1 PD earlier than the TE path signal, the overall output of the PD could be distorted if the input signal is at an arbitrary polarization state. However, as described in the next section, the receiver can tolerate a significant amount of delay between the two orthogonal signals, before the bit error rate (BER) starts to deteriorate.

A floating germanium PD [15] design is used due to its low dark current, high responsivity, and large bandwidth. It consists of a 1.25 μm wide Ge deposition on top of a p-i-n doped rib waveguide, as shown in Fig. 2. The PD is sufficiently long (21μm) to absorb all of the incident light without letting any residual light pass through.

The microring filter parameters are listed in Table 2. Rib waveguides with core dimensions of 500nm width and 220nm thickness, and a slab thickness of 90nm, are used for the filters. Although the nominal channel spacing is set to 2.5nm, the ring filters can be tuned with metal heaters to accommodate a tighter channel spacing. The drop port gap is designed to be larger

Optics EXPRESS

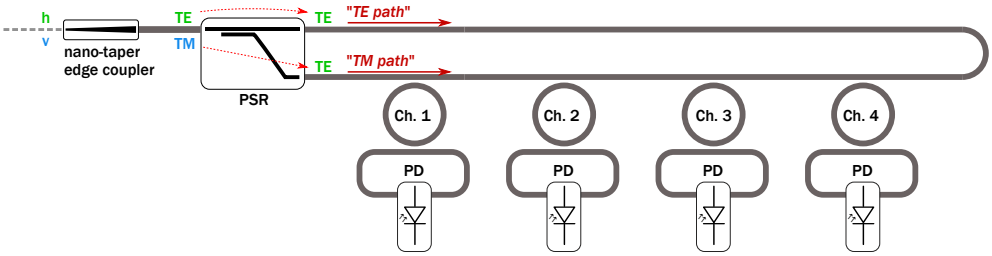

Fig. 1. Schematic of the 4-channel polarization diversity receiver.

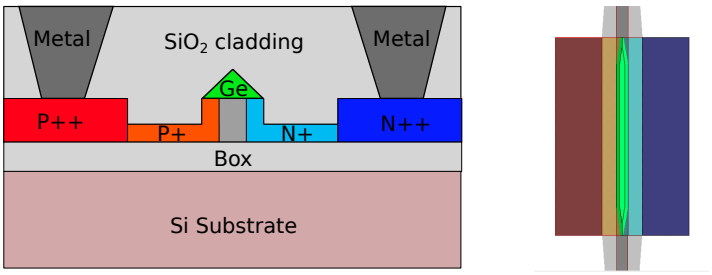

(a) (b)

Fig. 2. (a) Cross-sectional schematic of the floating Ge photodetector [15]. (b) Top view schematic of the photodetector.

than the through port gap to meet the critical coupling condition defined in [16] for maximum power transfer through the filter. However, the measured propagation loss within the microring filter turns out to be less than what was initially expected, which means the two gap distances need to be closer to one another.

Table 2. 4 Channel microring filter parameters

Diameter [μm]	20.00, 20.05, 20.10, 20.15
Through port gap [nm]	300
Drop port gap [nm]	320
Free Spectral Range [nm]	10
Channel Spacing [nm]	2.5
Quality Factor	15000

3. Device measurement

A test structure layout and an optical micrograph of the fabricated device are shown in Fig. 3. A coplanar GSG probe is used to measure the output of the PDs. The device is fabricated at the A*STAR Institute of Microelectronics (IME) foundry. The fabricated sample exhibits 1.5 dB/cm propagation loss in the waveguide, and cross coupling coefficients of approximately 0.19 and 0.17 at the microring filters' through port gap and drop port gap, respectively.

The through-port spectrum of the 4-channel WDM receiver is shown in Fig. 4(a). The spectrum is obtained by using an external PSR to separate the input and the output path, as shown

Optics EXPRESS

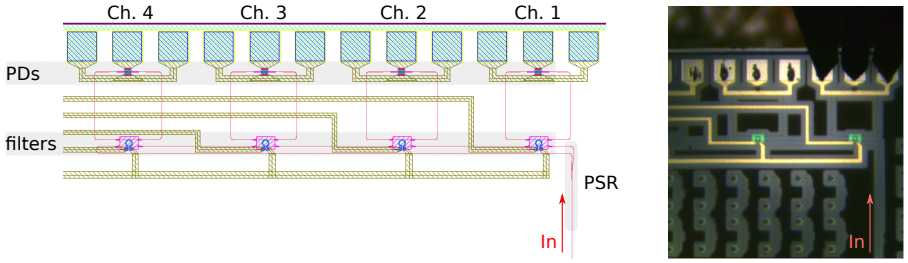

(a) (b)

Fig. 3. (a) Layout of the receiver. (b) Micrograph of the receiver, showing the PDs and ring filters for channels 1 and 2, and the PSR.

in Fig. 5. Due to multiple sources of reflections along the beam path, the spectrum contains multiple fringes. A duplicate measurement is also made by swapping the ports for the laser and the detector, resulting in a similar spectrum with minor differences in the fringe patterns. A typical quality factor of 15000 (±500) is observed across the chip. Metal heaters on top of each ring resonator can tune the resonant wavelength of each channel filter with 0.138nm/mW tuning efficiency. These heaters can compensate manufacturing variability which leads to variations in the central wavelength of each channel as well as variations in the spacing between channels [17].

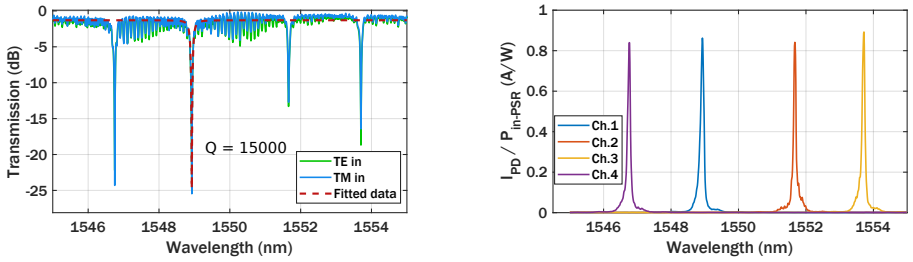

(a) (b)

Fig. 4. (a) Through-port spectrum of the receiver, (b) Output current spectrum at each PD, normalized to the input power at the PSR.

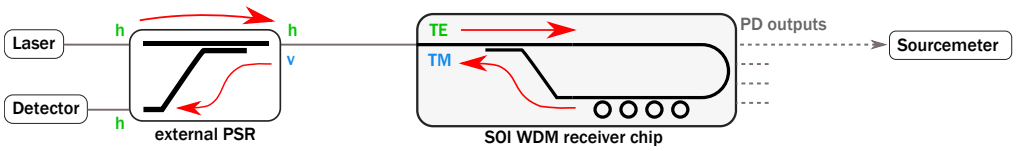

Fig. 5. Measurement setup for the through-port transmission spectrum of the receiver chip and the output current spectrum at each PD.

The wavelength dependent responsivity of the WDM channel filters is derived from measurement of the photocurrent in the PDs as a function of the on-chip optical power before the PSR (Fig. 4(b)). Normalization to the input power at the on-chip PSR is done in order to exclude the coupling losses from the edge coupler and the alignment errors, which contribute approximately 4.5-5.5 dB insertion loss with TE input. The PSR has a 0.4 dB insertion loss with negligible PDL, leading to a total of about 5.5-6.5 dB insertion loss from edge coupler to PD with TE input, including the propagation loss of the waveguides. The total insertion loss with TM input is 6.5-7.5 dB due to the PDL of the edge coupler. At a reverse bias voltage of 6 V, the average

Optics EXPRESS

responsivity of the PDs is 1.05 A/W, with an average dark current of 1.2 μA. The -3 dB bandwidth of the PD is measured to be >16 GHz, which is sufficiently large for measuring 10 Gb/s data.

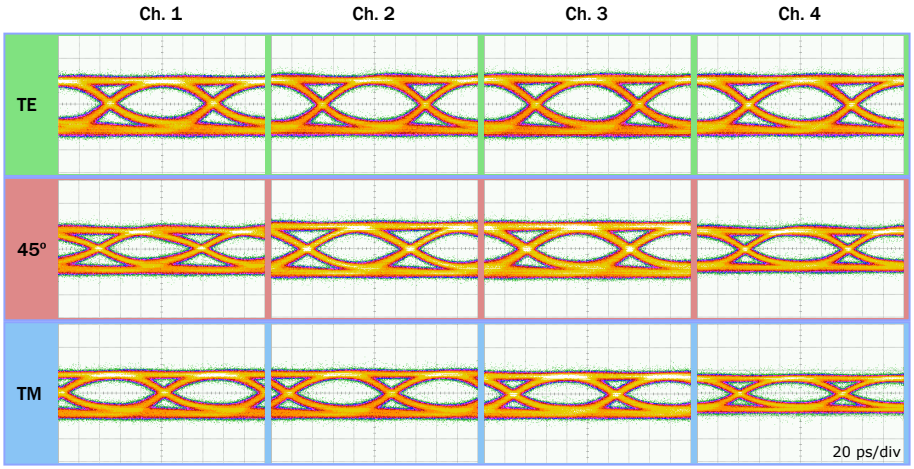

Fig. 6. Measured eye diagrams for the four channels at different input polarization states.

The 10 Gb/s eye diagram for each channel is presented in Fig. 6, obtained from the setup in Fig. 7. Pulse Pattern Generators (PPGs) provide non-return-to-zero (NRZ) 2^{31} - 1 pseudo random binary sequence (PRBS) signals to the 10 GHz $LiNbO_3$ Mach Zehnder modulators (MZMs) to generate 10 Gb/s modulated optical signals. The output of each MZM passes through a polarization controller and an off-chip multiplexer (MUX), which consists of two cascaded 3dB couplers, before entering the chip. The resonant wavelength of each channel is tuned by applying current to the metal heater on top of each ring filter. The response from the PD passes through a bias tee, and the RF output goes to either the oscilloscope for eye diagram measurement, or the error detector (ED) for BER measurement. A 15 GHz RF amplifier is placed before the ED due to the minimum peak-to-peak voltage requirement of the instrument. Due to limitations of our instrumentation, only up to three channels are simultaneously tested.

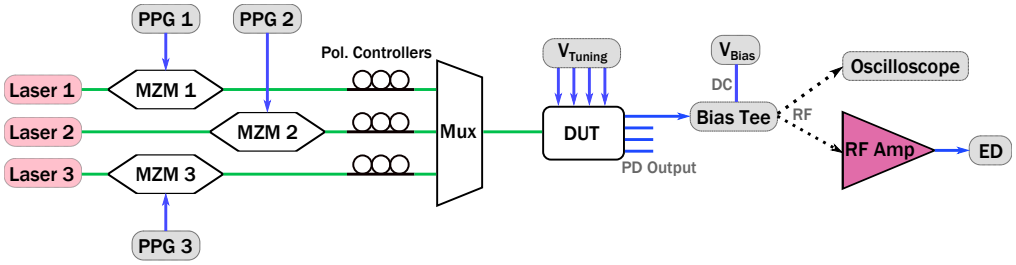

Fig. 7. Measurement setup for the eye diagram and bit error rate testing.

The eye diagrams for the three different input polarization states of TE, TM, and 45° on chip are obtained by using a polarization controller, an axis rotating fiber, and a slow-axis (SA) polarizer to maximize the response for the h, v, and 45° polarizations in the fiber respectively. For example, to align the output to h, a slow-axis polarizer is placed in the beam path, and the polarization controller is tuned until the output is maximized (Fig. 8(a)). For v alignment, a fast-axis to slow-axis (FA-to-SA) fiber is placed at the output of the polarizer, and once again the polarization controller is tuned to maximize the output (Fig. 8(b)). For 45° alignment, the

Optics EXPRESS

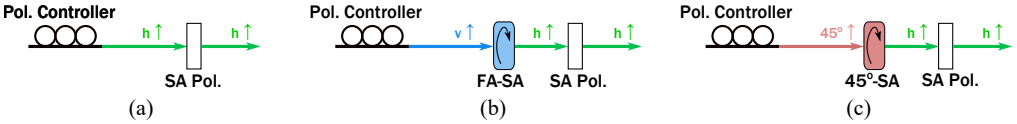

Fig. 8. Alignment setup for each polarization input. By maximizing the h polarization output after the SA polarizer, the output of the polarization controller is aligned to (a) h, (b) v, and (c) 45° polarizations.

FA-to-SA fiber is replaced with a 45°-to-SA fiber (Fig. 8(c)). After each alignment step, the slow-axis polarizer and the polarization rotating fiber (if used) are carefully removed from the link, which ensures that the propagation delay through those components are not added to the link. This is important for eye diagram assessment of this receiver.

The eye diagrams in Fig. 6 reveal a clear time delay between TE and TM input signals, as predicted in Section 2. The delay between TE and TM signals are 44ps, 32ps, 20ps, and 8ps (± 2ps) for channels 1, 2, 3, and 4, respectively. The amplitude difference between the TE and TM eyes primarily comes from the edge coupler, which exhibits PDL of approximately 1 dB. It should be noted that the reduced eye amplitude in channel 4 TM polarization is due to an alignment error from the polarization alignment step during the measurement. Nevertheless, clear eye diagrams are obtained for all states, including the mixed polarization states labeled as "45°". Although only the 45° data is shown, open eye diagrams at other polarization angles are also experimentally verified. All eye diagrams are round, except for the 45° eye for channel 1 which has sharper corners at the top and bottom. Eye diagrams at 45° polarization represent an equal weight sum of the TE and TM signals, and the sharp corners in the eye diagram arise as a result of a large delay between the two signals. This is clearly visible in Fig. 9, which shows the summation and relative time delay of simulated TE and TM pulses in channels 1 and 4. Fig. 9(a) shows a sharper peak at the top of the summed signal, with a slightly reduced pulse amplitude compared to Fig. 9(b). This leads to reduced height and width in the eye diagram of the summed signal.

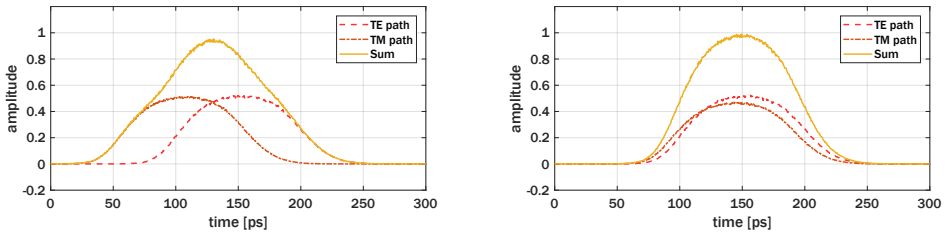

Fig. 9. Normalized sum of the TE and TM signals with a delay between them, corresponding to (a) channel 1 and (b) channel 4.

As shown in Fig. 10, similar eye diagrams are obtained through simulation using Lumerical Interconnect. The input signal is modeled as an amplitude modulated signal with 40 ps rise time and fall time. The PD for each channel is represented as two separate PDs - one for each direction of the input beam, with their outputs added in the electrical domain. A random jitter corresponding to 2% of the unit interval (UI) is added to the electrical input of the modulator, and a noise source with a power spectral density of 5e-20 W/Hz is added to the output sum of the PDs, to match the noise level in the measured eye diagrams. The TE-TM delay shifts by 12.5 ps between adjacent channels, which agrees with the measured data.

Optics EXPRESS

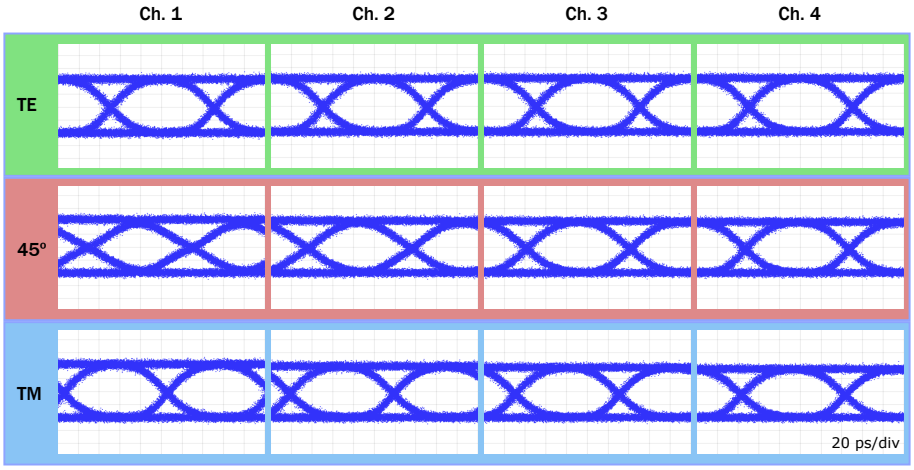

Fig. 10. Simulated eye diagrams for the four channels at different input polarization states.

The BER measurement results are presented in Fig. 11. With the PDL from the edge coupler properly calibrated using reference structures, the measured BERs are virtually indistinguishable for TE, TM, and 45° polarizations. The only case with a clear difference across all input powers is the 45° BER for channel 1, which has the largest delay between the signals in the TE path and the TM path.

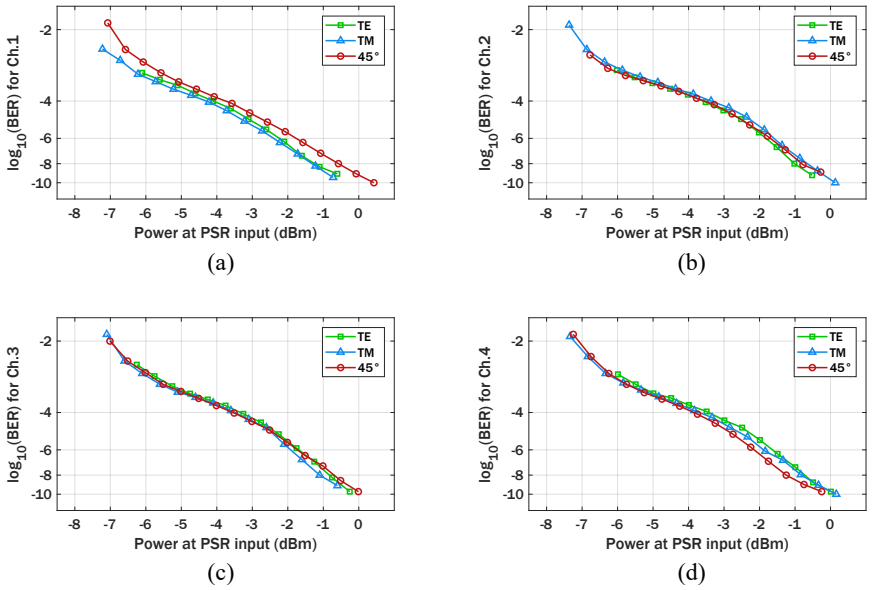

Fig. 11. BER measurements with TE, TM, and 45° polarization input, for channel (a) 1, (b) 2, (c) 3, and (d) 4.

At the nominal channel spacing of 2.5 nm, due to the high Q-factor and large channel spacing, the crosstalk between adjacent channels is negligible. To determine the receiver's applicability in a DWDM system, the spacing between channel 3 and channel 4 is tuned from 2.5nm down to 0.4nm (50.0 GHz), 0.3nm (37.5 GHz), and 0.2nm (25 GHz). The tuned spectra for 0.4

Optics EXPRESS

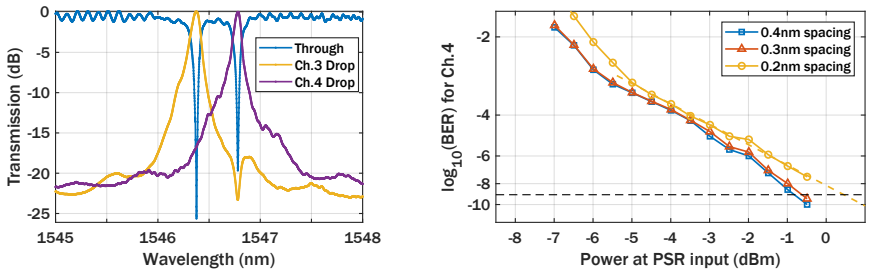

(a) (b)

Fig. 12. (a) Transmission spectrum of the receiver where channel 3's resonance is tuned to be 0.4nm away from channel 4's resonance. (b) BER measurement results at channel 4 PD, where the adjacent channel is tuned to be 0.4nm, 0.3nm, and 0.2nm away.

nm spacing and the BER data at the different spacings are plotted in Fig. 12. The horizontal polarization input is used for testing. Because the signal for channel 4 gets dropped first along the TE path, channel 3 only experiences a small amount of crosstalk from channel 4. Therefore, for the crosstalk assessment with the BER plot, only channel 4 is measured [18, 19]. Adjacent channel isolation between channel 3 and channel 4 are 17 dB, 14 dB, and 11 dB, for channel spacings of 0.4nm, 0.3nm, and 0.2nm, respectively.

The power penalty from the inter-channel crosstalk is quantified as the additional input power required to achieve a BER of 1e-9, in comparison to the case without any crosstalk. The BER values at 2.5nm spacing remain the same down to 0.4nm spacing. At 0.3nm spacing, there is a small change, resulting in 0.2 dB power penalty. At 0.2nm spacing, the crosstalk significantly increases, resulting in 1.0 dB power penalty. The progressive degradation in the eye diagrams shown in Fig. 13 is due to the effects of the crosstalk.

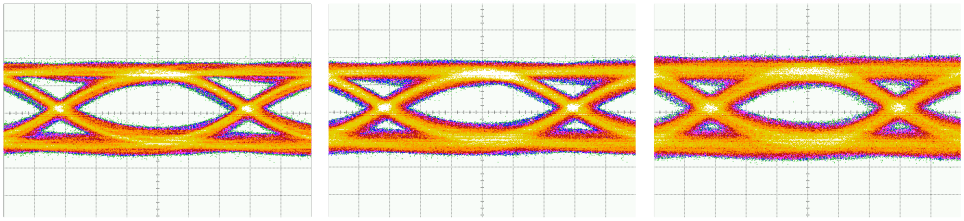

(a) (b) (c)

Fig. 13. Measured eye diagrams for channel 4, with channel spacing of (a) 0.4nm, (b) 0.3nm, and (c) 0.2nm.

4. Discussion

The BER measurement at the 45° polarization state indicates that a 10Gb/s signal, which translates to a UI of 100ps, can withstand up to at least 32ps of delay between the TE and TM signals without impairment. The 32ps delay corresponds to about 2200μm difference in the strip waveguide path. This BER tolerance to TE-TM signal delay implies that optical delay lines, as suggested in [10], are in fact not necessary to fine tune the optical path lengths, provided the TE-TM delay is less than 30% of the UI. For each receiver channel, the waveguide between the ring filter and the PD can be adjusted such that the total TE signal path and the TM signal path leading to the PD are nominally equal in length. Due to the large tolerance for path length difference, the receiver performance should remain unaffected against on-chip variation of waveguide dimensions.

Optics EXPRESS

Because the BER measurement is performed at the optimal decision point in each eye diagram, only the eye height, and not the eye width, is taken into consideration for this delay tolerance assessment, assuming reasonably open eyes (eye widths). This is a valid assumption, as the clock and data recovery (CDR) circuits implemented in commercial receivers [20] can always tune themselves to the optimal decision point, and thus compensate for any slow polarization change in the single mode fiber. The TE-TM delay tolerance will scale with the UI of the modulated signal. For example, a 50 Gb/s signal (UI = 20ps) will withstand up to 6.4ps of TE-TM delay, corresponding to about 440μm strip waveguide path length difference. This may be significantly smaller than the tolerable path length difference for a 10 Gb/s signal, but it is still sufficiently large that on-chip tunable delay lines will not be necessary.

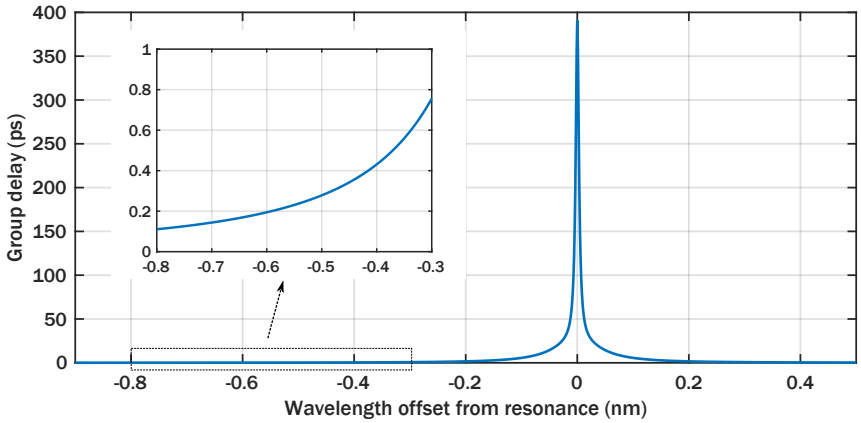

Fig. 14. Through-port group delay vs. wavelength for a single ring filter.

For DWDM application, each add-drop ring filter may add a group delay to the propagating signal, which could potentially worsen the TE-TM delay for the receiver. For example, the add-drop filters used in this work can theoretically add up to 390ps of group delay close to resonance, as shown in Fig. 14. However, the group delay is significantly reduced to only 0.4ps at 0.4nm offset from resonance, and it gets smaller with increasing offset from resonance. Assuming a total of 25 DWDM channels with 0.4nm spacing, which can be accommodated for ring filters with an FSR of 10nm, a signal can accumulate up to 1.4ps of additional group delay as it passes through the 24 other channel filters, before arriving at the target channel filter. This value is small in comparison to the aforementioned 32ps tolerance for TE-TM delay. Therefore, the group delay from each ring filter will not pose a major problem to the receiver performance in a DWDM link.

Due to the waveguide loop in the design, there is a risk of high return loss back to the input of the receiver. For example, assuming all channel filter resonances are perfectly aligned to the input laser wavelengths, a high return loss of -12dB can be expected from one of the channels in Fig. 4(a). This value can be improved by correct design and a stable manufacturing process, as the best-case scenario in Fig. 4(a) shows a much lower -25 dB return loss. These values do not include the insertion loss from the edge coupler, which would further reduce the total return loss.

The large quality factor of 15000 is chosen to minimize inter-channel crosstalk for 10 Gb/s operation in this work. However, for the performance of each channel, a small quality factor is preferred, not just due to the optical bandwidth from the photon lifetime limit, but also due to the tolerance for high input power. In a high-Q ring, the optical power can build up within the ring, leading to resonance shift from the self-heating effect [21], Kerr nonlinearity and two-photon absorption, when high optical input power is applied. This power-dependent resonance shift can lead to degradation of the modulated signal and may limit the maximum signal-to-noise ratio

Optics EXPRESS

possible, which is why the importance of resonance stabilization is emphasized in [21] as well. Furthermore, this resonant shift can lead to increased return loss back to the input of the receiver, as the fraction of light coupled into each channel is reduced. Since the photodetector response in each channel does not benefit from the optical power build-up within the ring filters, it is best to use higher-order ring filters with low quality factor to ensure high input power tolerance while keeping the inter-channel crosstalk low.

5. Conclusion

The operation of a 4-channel WDM polarization insensitive receiver based on microring resonator filters and a looped PSR is demonstrated at 10Gb/s per channel. Large signal measurements at TE, TM, and 45° polarization states show that each channel can tolerate up to 32ps delay between the TE and TM signals before the BER degrades at an arbitrary polarization. This indicates the receiver's robustness against on-chip variations. Furthermore, the large signal measurements at reduced channel spacings indicate that the inter-channel crosstalk is negligible down to 0.4nm spacing, thus demonstrating its compatibility for DWDM operation.

Funding

Networks of Centres of Excellence of Canada; Natural Sciences and Engineering Research Council of Canada

Acknowledgments

We would like to thank Prof. Nicolas A.F. Jaeger for assistance with laboratory equipment and measurements. We thank the Refined Manufacturing Acceleration Process (ReMAP) network, part of Canada's Business-led Networks of Centres of Excellence, and Natural Sciences and Engineering Research Council of Canada for funding, and Christine Alain and Alex Paquet at INO, Robert Suurmann and Tatiana Berdinskikh at Celestica, Robert Mallard at CMC Microsystems, and Odile Liboiron-Ladouceur at McGill University for discussions.

References

1. A. H. Ahmed, A. Sharkia, B. Casper, S. Mirabbasi, and S. Shekhar, "Silicon-photonics microring links for datacenters – challenges and opportunities," IEEE J. Sel. Top. Quantum Electron. **22**, 194–203 (2016).
2. D. Y. Lee, X. Zheng, J. Yao, Y. Luo, J.-H. Lee, S. Lin, H. Thacker, J. Bovington, I. Shubin, S. S. Djordjevic, J. E. Cunningham, K. Raj, and A. V. Krishnamoorthy, "Error-free operation of a polarization-insensitive 4λ x 25 Gbps silicon photonic WDM receiver with closed-loop thermal stabilization of Si microrings," Opt. express **24**, 13204–13209 (2016).
3. Z. Lu, Y. Wang, F. Zhang, N. A. Jaeger, and L. Chrostowski, "Wideband silicon photonic polarization beamsplitter based on point-symmetric cascaded broadband couplers," Opt. express **23**, 29413–29422 (2015).
4. Z. Lu, M. Ma, H. Yun, Y. Wang, N. A. Jaeger, and L. Chrostowski, "Silicon photonic polarization beamsplitter and rotator for on-chip polarization control," in *IEEE Int. Conf. Group IV Photonics,* (2016), pp. 70–71.
5. Y. Xu and J. Xiao, "Ultracompact and high efficient silicon-based polarization splitter-rotator using a partially-etched subwavelength grating coupler," Sci. reports **6**, 27949 (2016).
6. A. Xie, L. Zhou, J. Chen, and X. Li, "Efficient silicon polarization rotator based on mode-hybridization in a double-stair waveguide," Opt. express **23**, 3960–3970 (2015).
7. Y. Ma, Y. Liu, H. Guan, A. Gazman, Q. Li, R. Ding, Y. Li, K. Bergman, T. Baehr-Jones, and M. Hochberg, "Symmetrical polarization splitter/rotator design and application in a polarization insensitive wdm receiver," Opt. express **23**, 16052–16062 (2015).
8. P. De Heyn, J. De Coster, P. Verheyen, G. Lepage, M. Pantouvaki, P. Absil, W. Bogaerts, D. Van Thourhout, and J. Van Campenhout, "Polarization-insensitive 5x20gb/s wdm ge receiver using compact si ring filters with collective thermal tuning," in *Optical Fiber Communication Conference,* (Optical Society of America, 2014), pp. Th4C–5.
9. L. Chen, C. R. Doerr, and Y.-k. Chen, "Polarization-diversified dwdm receiver on silicon free of polarization-dependent wavelength shift," in *Optical Fiber Communication Conference,* (Optical Society of America, 2012), pp. OW3G–7.
10. H. Fukuda, K. Yamada, T. Tsuchizawa, T. Watanabe, H. Shinojima, and S.-i. Itabashi, "Silicon photonic circuit with polarization diversity," Opt. express **16**, 4872–4880 (2008).

Optics EXPRESS

11. J. Zhang, H. Zhang, S. Chen, M. Yu, G. Q. Lo, and D. L. Kwong, "A tunable polarization diversity silicon photonics filter," Opt. express **19**, 13063–13072 (2011).
12. Y. Tan, H. Wu, and D. Dai, "Silicon-based hybrid (de) multiplexer for wavelength-/polarization-division-multiplexing," IEEE J. Light. Technol. **36**, 2051–2058 (2018).
13. W. D. Sacher, T. Barwicz, B. J. Taylor, and J. K. Poon, "Polarization rotator-splitters in standard active silicon photonics platforms," Opt. express **22**, 3777–3786 (2014).
14. R. Gatdula, K. Kim, A. Melikyan, Y.-K. Chen, and P. Dong, "Simultaneous four-channel thermal adaptation of polarization insensitive silicon photonics WDM receiver," Opt. express **25**, 27119–27126 (2017).
15. Y. Zhang, S. Yang, Y. Yang, M. Gould, N. Ophir, A. E.-J. Lim, G.-Q. Lo, P. Magill, K. Bergman, T. Baehr-Jones, and M. Hochberg, "A high-responsivity photodetector absent metal-germanium direct contact," Opt. express **22**, 11367–11375 (2014).
16. W. Bogaerts, P. De Heyn, T. Van Vaerenbergh, K. De Vos, S. Kumar Selvaraja, T. Claes, P. Dumon, P. Bienstman, D. Van Thourhout, and R. Baets, "Silicon microring resonators," Laser & Photonics Rev. **6**, 47–73 (2012).
17. Z. Lu, J. Jhoja, J. Klein, X. Wang, A. Liu, J. Flueckiger, J. Pond, and L. Chrostowski, "Performance prediction for silicon photonics integrated circuits with layout-dependent correlated manufacturing variability," Opt. express **25**, 9712–9733 (2017).
18. H. Jayatilleka, K. Murray, M. Caverley, N. A. Jaeger, L. Chrostowski, and S. Shekhar, "Crosstalk in SOI microring resonator-based filters," IEEE J. Light. Technol. **34**, 2886–2896 (2016).
19. M. Bahadori, S. Rumley, H. Jayatilleka, K. Murray, N. A. Jaeger, L. Chrostowski, S. Shekhar, and K. Bergman, "Crosstalk penalty in microring-based silicon photonic interconnect systems," IEEE J. Light. Technol. **34**, 4043–4052 (2016).
20. J. Jaussi, G. Balamurugan, S. Hyvonen, T.-C. Hsueh, T. Musah, G. Keskin, S. Shekhar, J. Kennedy, S. Sen, R. Inti, M. Mansuri, M. Leddige, B. Horine, C. Roberts, R. Mooney, and B. Casper, "A 205mW 32Gb/s 3-tap FFE/6-tap DFE bidirectional serial link in 22nm CMOS," in *IEEE Int. Solid-State Circuits Conf.*, (2014), pp. 440–441.
21. C. Sun, M. Wade, M. Georgas, S. Lin, L. Alloatti, B. Moss, R. Kumar, A. H. Atabaki, F. Pavanello, J. M. Shainline, J. S. Orcutt, R. J. Ram, M. Popović, and V. Stojanović, "A 45 nm cmos-soi monolithic photonics platform with bit-statistics-based resonant microring thermal tuning," IEEE J. Solid-State Circuits **51**, 893–907 (2016).